Low-Loss Polytetrafluoroethylene Hexagonal Porous Fiber for Terahertz Pulse Transmission in the 6G Mobile Communication Window

Yong Soo Lee, Hyucksu Choi, Byungjoo Kim, Chul Kang, Inhee Maeng, Seung Jae Oh, Soeun Kim, and Kyunghwan Oh

***Abstract*— Hexagonal porous optical fiber without a central defect is proposed and numerically analyzed with the finite element method (FEM) for transmitting terahertz (THz) electromagnetic wave pulse. In experiments, the transmission characteristics of polytetrafluoroethylene (PTFE) hexagonal porous optical fibers were measured using a THz time-domain spectroscopy (THz-TDS) system. To precisely estimate the effective material loss (EML), we measured the refractive index and absorption coefficient of PTFE in the THz range to use them in FEM analyses, and the EML of the porous fiber was estimated to be lower than that of a bulk rod as large as by a factor of 2 in the frequency range from 0.1 to 0.33 THz. In experiments, we measured the transmission characteristics of both the porous fibers and the bulk rod, to confirm a significant improvement in THz wave transmission nearly by an order of magnitude in the 6G telecommunication window, showing a better performance than theoretical estimations.**

***Index Terms*— Optical waveguide, porous fiber, 6G telecommunication window, terahertz (THz).**

I. Introduction

OVER the decades, technological advances in the generation and detection of terahertz (THz) waves have continued rapidly, and continuous-wave (CW) THz sources are commercially available presently [1], [2], along with complete THz spectroscopy and imaging systems in the market [3]–[5]. Since the THz band covers both electronic and optical regions, there have been continuous efforts to further extend the frequency range in optical component design toward THz, taking advantage of well-established photonic technologies. Significantly, the THz band from 0.1 to 0.3 THz has been a vital research interest in recent years since it is considered the main transmission band for 6G telecommunication [6], [7] and a radar band for autonomous vehicles [8]. These technologies based on THz communication and sensing would play a key role in establishing future social infrastructure providing intelligent services such as 4K high-definition services, virtual reality, augmented reality, the internet of things (IoT), and unmanned vehicle maneuvering. Recently, with the development of IoT and the rapid increase in communication bandwidth demand, 5G band communication has been commercialized worldwide. Furthermore, 6G is already being discussed for the following services, and various studies for THz communication near 0.3 THz have been recently reported [6], [7], [9]–[11]. Most THz systems still rely on free-space propagation technologies, which inherently suffer from atmospheric attenuation by water vapor and oxygen molecules. To overcome the free-space propagation limitations, THz waveguide technology has been intensively studied for several decades such as parallel plate, slit waveguide, and bare metal wire [12]–[14] in a metallic waveguide and index-guiding and photonic bandgap fiber [15]–[25] in a dielectric waveguide. Especially, low-loss short-length THz waveguides to interconnect transmitters and receivers in high-performance chips are being reported to take advantage of the THz waveguide allowing higher electromagnetic wave energy to reach the receiver than free-space propagation [9]–[11]. As an early attempt, metal wire and metal-coated dielectric tubes have been proposed for THz waveguides. However, they suffer from a high bending loss and a low efficiency of bonding to embedding materials [13], [14]. As an alternative, polymer-based bandgap fibers, Bragg fibers, hollow core fibers, and solid core fibers have been reported [15]–[25] to take advantage of the relatively low absorption of specific polymers in the THz range. However, prior studies have confirmed that a significant amount of the guided mode should propagate into the air to achieve a sufficiently low propagation loss regardless of the absorption of waveguide materials [19]–[25].

Recently, porous core fibers and photonic crystal fibers (PCFs) with central defects have been proposed to substantially increase the air fraction of the guided mode for

Manuscript received April 13, 2021; revised May 30, 2021; accepted June 9, 2021. Date of publication September 30, 2021; date of current version November 4, 2021. This work was supported in part by the National Research Foundation of Korea (NRF) funded by the Ministry of Education under Grant 2018R1D1A1B07049349 and in part by the NRF grant funded by the Ministry of Science and ICT (MSIT) of the Korea Government under Grant 2019R1A2C2011293. *(Corresponding authors: Kyunghwan Oh; Soeun Kim.)*

Yong Soo Lee, Hyucksu Choi, Byungjoo Kim, and Kyunghwan Oh are with the Department of Physics, Yonsei University, Seoul 03722, South Korea (e-mail: xylys@yonsei.ac.kr; sciench1@yonsei.ac.kr; byungjookim@yonsei.ac.kr; koh@yonsei.ac.kr).

Chul Kang and Soeun Kim are with the Integrated Optics Laboratory, Advanced Photonics Research Institute, GIST, Gwangju 61005, South Korea (e-mail: iron74@gist.ac.kr; sekim@gist.ac.kr).

Inhee Maeng and Seung Jae Oh are with the YUHS-KRIBB Medical Convergence Research Institute, College of Medicine, Yonsei University, Seoul 03722, South Korea (e-mail: inheem@yonsei.ac.kr; u95slj@yonsei.ac.kr).

Color versions of one or more figures in this article are available at https://doi.org/10.1109/TMTT.2021.3092761.

Digital Object Identifier 10.1109/TMTT.2021.3092761

further reducing the waveguide loss in THz bands [21]–[25]. However, since the solid core propagates light into the material region, this is accompanied by high material absorption. In contrast, porous cores can reduce material absorption and consequently transmission losses. In porous core fibers, the polymer rod with air holes itself serves as the core while the surrounding air acts as the cladding. Thus, their structure effectively simplifies the fabrication process. In contrast, PCFs require a thick cladding layer to reduce confinement loss [27]. An increase in the air fraction and layers in PCFs results in an inevitable tradeoff between the modal guidance and fabrication difficulties. Therefore, porous core fibers are considered to provide more flexible control of the air fraction of the guided mode than PCFs.

In this study, we proposed a low-loss porous core fiber with high porosity of 40% for THz pulse transmission. The proposed optical fibers consisted of the porous core and the air cladding to guide the light by the total internal reflection similar to the waveguiding mechanism of a conventional optical fiber. By the air holes within the porous core, the transmission and dispersion properties can be further tailored in contrast to the conventional optical fibers. Its transmission characteristics were thoroughly investigated using a finite element method (FEM) package, COMSOL. In experiments, a porous fiber made of polytetrafluoroethylene (PTFE) with 19 air holes of subwavelength size arranged in a hexagonal lattice without central defects was investigated using a THz time-domain spectroscopy (THz-TDS) system to confirm its low propagation loss in the THz frequency range. We compared the porous core fiber with a solid rod of a similar outer diameter (O.D.) without air holes and experimentally confirmed substantial improvement in THz transmission loss by order of magnitude in the 6G telecommunication window, for the first time to the best knowledge of the authors.

II. Waveguide Structure and THz Measurements Set-Up

In recent years, applications of PTFE tubes in biochemical and pharmaceutical fields are rapidly increasing due to highly matured PTFE processing technology. Moreover, custom foundry services for specially designed tubes are available. Especially, a PTFE tubing with air holes can be extruded in a hot pressurized dye to maintain the air hole structures for a long tube length [28]–[30]. It is known that cyclic olefin copolymer (COC, TOPAS/ZEONEX) can provide a lower material loss than PTFE (TEFLON) for transmitting THz waves. However, PTFE has clear and practical advantages over other materials containing COC, especially in foundry services. PTFE processing technology has been highly advanced, and the current state of the art can provide a very high yield and uniformity even in delicate tubing structures. A photograph of the PTFE porous core fibers used in this study is shown in Fig. 1, custom-made [31]. The right inset is the cross section of the fiber. The porous core fiber consists of identical 19 air holes arranged in a hexagonal lattice structure without any central defects. Most of the prior porous core fibers had a defect structure at the center in a complex air hole arrangement that significantly differed from outer air holes [32], [33]. However, the complex central defect has cast the fundamental limitation in actual fabrication processes and its uniformity along the longitudinal direction. In our porous core fiber, in contrast to prior complicated defect structures, only three structural parameters are defined as shown in the right inset of Fig. 1; the air hole diameter (D), its pitch (Λ), and the O.D. Note that D is identical in all 19 air holes without the central defects, which can substantially alleviate the fabrication process and the uniformity issues compared with prior porous core fibers. In this study, we set $D = 430\ \mu$m, $\Lambda = 560\ \mu$m, and O.D. $= 3.0$ mm, and the porosity of this fiber was estimated to be $\sim$40%. The porous core fiber had a length of $\sim$20 cm, and the structural parameters showed negligible variations along the axial direction.

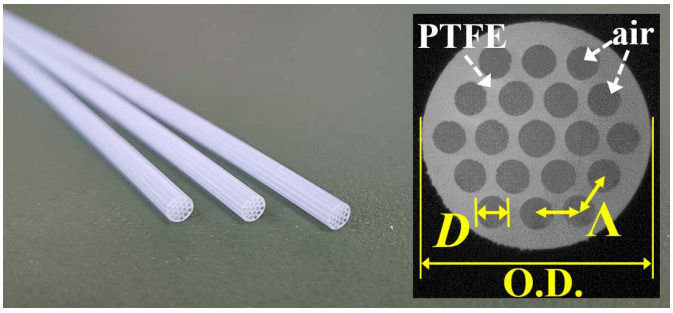

Fig. 1. Photograph and cross section of the porous core fiber made of PTFE. The porous fiber has 19 air holes arranged in a hexagonal lattice structure with the air hole diameter (D), the pitch (Λ), and the O.D.

To quantify the optical properties of PTFE in the THz band, we used a PTFE rod with a diameter of 3.0 mm, and its transmission was measured using a standard THz-TDS system [34]–[36] as schematically shown in Fig. 2(a). THz-TDS was based on a femtosecond Ti:sapphire laser (Mai Tai, Spectra-physics), which had the central wavelength at 800 nm, the pulse duration of $\sim$100 fs, and the pulse repetition rate of 80 MHz. The laser was divided into the THz generation arm and the detection arm by a beam splitter. One of the split laser beams was injected into InAs crystal to generate THz radiation. The emitted THz radiation was collimated and focused using parabolic mirrors to allow measurements in the spectral range from 0.1 to 1.6 THz. The waveguide sample (PTFE rod or PTFE porous core fiber) was mounted such that its ends were located at the focal positions of the parabolic mirrors on both sides. The transmitted pulse signal through the waveguide sample was detected using a photoconductive antenna. The fast Fourier processes acquired time-domain signals' transform (FFT) to obtain the frequency-domain signals. Due to the low dynamic range and high material loss in the waveguides at high frequencies, we only investigated the spectral range from 0.1 to 1.0 THz in this study. Fig. 2(b) shows the refractive index and the absorption coefficient of the PTFE rod with a length of 10.0 mm, which is the same material as the proposed porous core fiber in Fig. 1. The refractive index was measured to be 1.447 and was nearly constant in the entire

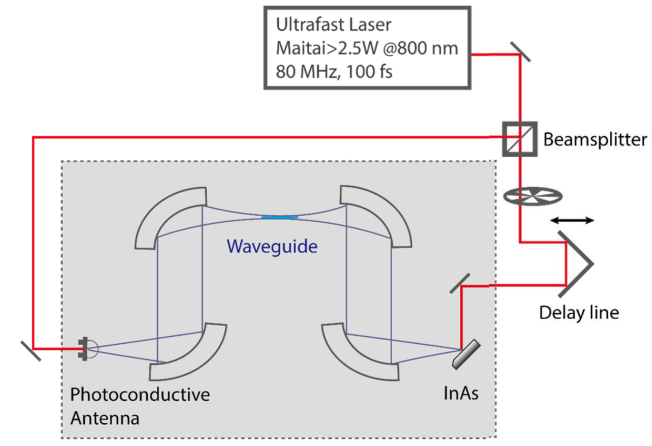

(a)

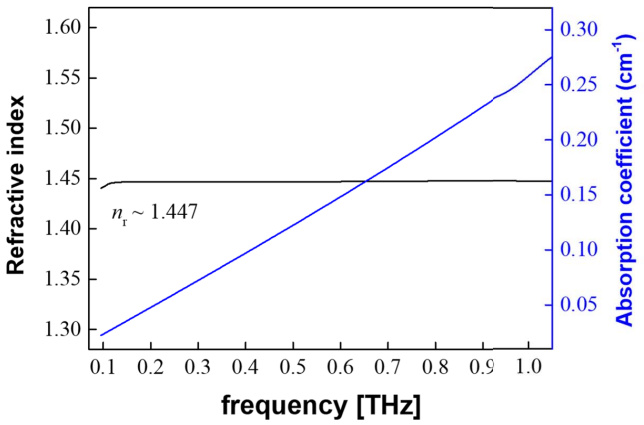

(b)

Fig. 2. (a) Experimental setup of THz time-domain spectroscopy. Here, the waveguide is either the PTFE rod or the proposed PTFE porous core fiber. (b) Measured refractive index and absorption coefficient of the PTFE rod.

frequency range. The absorption coefficient monotonically increased from 0.052 cm^{-1} at 0.1 THz to 0.257 cm^{-1} at 1.0 THz. This absorption coefficient is consistent with previous reports [27], and its variation was curve-fitted using the polynomial regression and used in the following numerical analyses.

III. Mode Analyses Using FEM and Estimation of Effective Material Loss

We numerically investigated two loss mechanisms; the effective material loss (EML, α_{mat}) and the confinement loss, as shown in Figs. 3 and 4, respectively. EML refers to the absorption loss that occurs in a material when light passes through an optical fiber, while the confinement loss occurs due to the leakage characteristics of the mode, affected by the number of air hole layers, their sizes, pitch, and their arrangement.

The EML can represent the effective optical loss of a guided mode, including the impacts of the air filling ratio. The EML, α_{eff}, was calculated using the following equation [37]:

$$\alpha_{eff} = \frac{(\varepsilon_0/\mu_0)^{1/2} \int_{A_{mat}} n\alpha_{mat}|E|^2 dA}{2\int_{All} S_z dA} \quad (1)$$

where ε_0 and μ_0 are the permittivity and the permeability of the vacuum, respectively. α_{mat} is the bulk material absorption loss of PTFE, and n is its refractive index. We used the experimental values for both α_{mat} and n in Fig. 2(b). The electric field E and Poynting vector $S_z = 1/2\mathrm{Re}(E \times H*)\hat{z}$ were calculated for the guided modes using an FEM package (COMSOL v5.4) in the THz frequency range. Here, we investigated the EML of three waveguide structures: a PTFE rod, a PTFE hexagonal PCF with a single defect at the center, and our proposed porous core fiber. For the numerical analysis, the COMSOL FEM package and the perfectly matched layer (PML) boundary condition were used. Here, the common structural parameters of fibers are O.D. = 3.0 mm, $\Lambda = 560$ μm, and D = 430 μm. In the simulation, the diameter of the air cladding and the thickness of the PML were 21 and 1.5 mm, respectively. The maximum mesh size was 200 μm in the core region, 300 μm in the cladding, and the meshes consisted of 29 688 triangular elements. The PTFE rod had no holes, while the PCF had the central defect in the same hexagonal air hole lattice as the proposed porous core fiber. The results are summarized in Fig. 3(a), where the normalized EML referenced to the material loss, $\alpha_{eff}/\alpha_{mat}$, was plotted as a function of frequency. The insets at the right-bottom are the intensity distributions of the fundamental mode at $f = 0.2$ THz, which shows that the porous core fiber guided the THz wave over a substantially larger number of air holes than others. When the THz wave propagates through the air holes, EML is expected to decrease because the absorption through the material is reduced. By including air holes, both PCF and the proposed porous core fiber showed a significant reduction in EML compared with bulk PTFE rod, and the proposed fiber showed a clear advantage over PCF in the lower frequency THz transmission since more of the THz waves interacted with air holes in the proposed fiber than PCF. See the inset of Fig. 3(a). As the frequency increased over 0.33 THz, we noted that the THz wave in the proposed fiber propagates mainly through PTFE rather than the air holes. We distinguished the THz wave guidance difference by solid and dashed blue lines in the line representing the porous fiber. It is divided into the solid line and the dashed line in the figure. In the potential 6G telecommunication band from 0.1 to 0.33 THz, the EML of the proposed porous fiber showed a meaningfully low value ranging from 0.01 to 0.07 cm^{-1}. Especially at the frequency of 0.2 THz, the EML of the proposed fiber 0.031 cm^{-1} was reduced by more than a factor of 2 from 0.072 cm^{-1} in the bulk rod. The THz wave propagates mostly through PTFE material in the higher frequency, and therefore EML of PCF and the proposed fiber converged to that of PTFE rod.

Confirming the lowest propagation loss in the proposed fiber in Fig. 3(a), we further investigated how EML would be affected by varying the number of air hole layers. To further quantify the THz wave propagation through the proposed

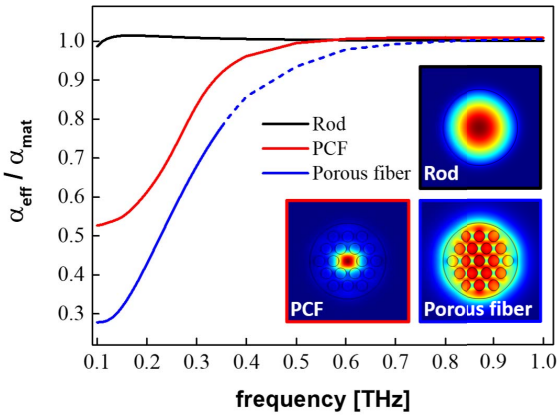

(a)

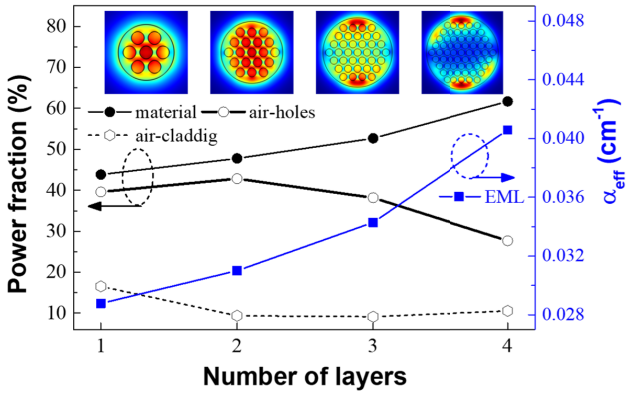

(b)

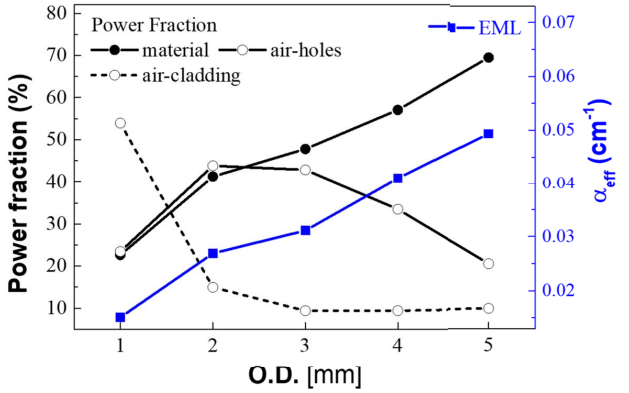

(c)

Fig. 3. (a) EML for different structures with the same structure parameters with O.D. = 3 mm, $\Lambda = 560$ μm, and $D = 430$ μm fixed. The insets are modal distributions of fundamental mode at 0.2 THz by fiber types. (b) EML and power fraction for four different layers with $\Lambda = 560$ μm and $D = 430$ μm fixed. The insets are modal distributions of fundamental mode at 0.2 THz depending on the number of layers. (c) EML and power fraction as a function of O.D. with D/Λ fixed to 0.77.

porous fiber, we defined "power fraction ratio" as below:

$$\text{Power fraction} = \frac{\int_X S_z dA}{\int_{\text{All}} S_z dA} \tag{2}$$

where the denominator is the integration for all the areas, while the numerator is for the area of interests denoted by X. We investigated three areas of interest, PTFE material, air holes in the porous core, and air cladding. Increasing the air hole layer numbers from 1 to 4, we calculated the power fractions and EML for the fundamental mode keeping the structural parameters $\Lambda = 560$ μm and $D = 430$ μm. The results are summarized in Fig. 3(b), and the insets at the top are intensity distributions of the fundamental mode at 0.2 THz for the corresponding number of air hole layers in the bottom horizontal axis. As shown in the insets, the guided mode rapidly spread toward the PTFE edge of the fiber as the number of air hole layers increased, and consequently increased EML. With the parameter mentioned above, the power fraction in the air hole region was the largest when the porous core had two air hole layers. See the data in open circles in Fig. 3(b). As adding more air hole layers, the THz wave was more confined to the material on the fiber edge, consistent with the inset figures. In the case with only one layer, the power fraction in the air cladding increased, which can cause additional transmission losses due to bending or external influences. We also investigated how the power fraction changed with the O.D. of the fiber. The results calculated at 0.2 THz are summarized in Fig. 3(c). Here, O.D. varied from 1 'to 5 mm, while the air filling ratio, D/Λ, was fixed to 0.77. At O.D. = 3 mm, the power fraction in the air cladding region reached a minimum, 9.4%. Note that when O.D. is 3 mm, the transmission loss due to external influences, which has been a major concern in prior waveguide designs, can be minimized as well. However, if O.D. further increased, the THz wave was more confined to the material on the fiber edge, and thus the net EML increased.

Since the higher order modes have significantly larger EMLs than the fundamental mode, the single-mode guidance can be achieved by controlling the fiber length or by bending. On the other hand, in Fig. 3(c) as the O.D. decreases, the power fraction of air cladding increases significantly, which can induce optical loss by the interaction between the light in the air cladding and external environmental absorption. Therefore, regarding the pure single-mode operation, the fiber diameter should be further optimized to confine the mode within the porous core, which is being pursued by the authors.

We varied the air filling ratio, D/Λ, from 0.5 to 0.9 to investigate its impacts on EML in the proposed fiber. Here, we fixed O.D. = 3.0 mm and $\Lambda = 560$ μm. The analysis results are summarized in Fig. 4(a). As D/Λ increases, the area of the air holes further increases to result in a reduction in EML. However, in the larger D/Λ, the fundamental mode cutoff appears, and the THz wave is no longer guided into the air holes like porous core. The vertical arrows in Fig. 4(a) mark the cutoff frequency for the given D/Λ. When D/Λ was less than 0.6, we did not observe the cutoff in the frequency range from 0.1 to 0.5 THz. Considering both EML and the fundamental modal guidance in the 6G band, we found $D/\Lambda = 0.77$ was optimal.

For the structural parameters ($\Lambda = 560$ μm, $D/\Lambda = 0.77$, O.D. = 3.0 mm), we calculated the confinement loss, L_c,

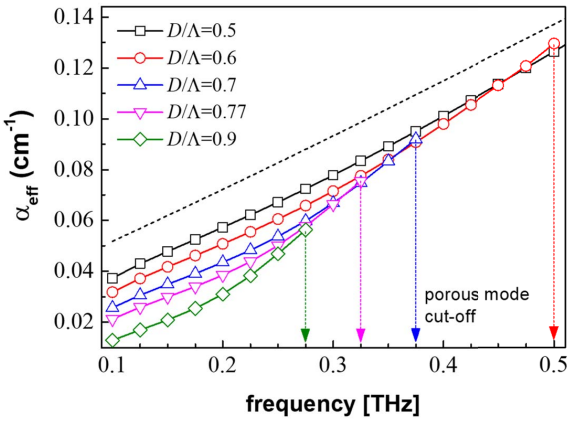

(a)

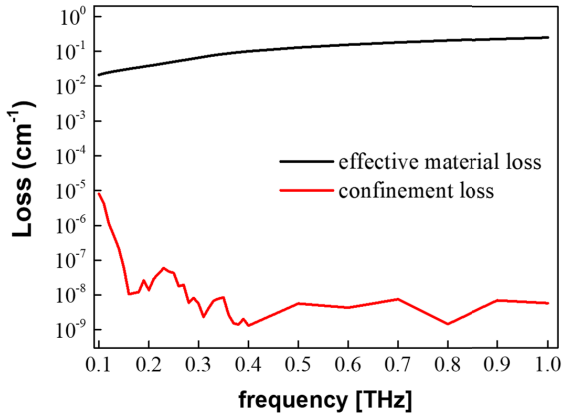

(b)

Fig. 4. (a) EML in the proposed porous core fiber for various air filling ratios (D/Λ). (b) EML and the confinement loss as a function of THz frequency.

of the porous fiber using the following equations [37]:

$$L_c = \left(\frac{4\pi f}{c}\right)\mathrm{Im}(n_{\mathrm{eff}})\ \mathrm{cm}^{-1} \tag{3}$$

where $\mathrm{Im}(n_{\mathrm{eff}})$ is the imaginary part of the complex effective index of the fundamental mode, f the operating frequency, and c the speed of light. Note that the unit of confinement loss is cm^{-1} and can be directly compared with EML as in Fig. 4(b). In the porous core fiber, the air serves as the cladding with a large refractive index contrast, and the confinement loss is orders of magnitude lower than EML. Therefore, EML is a decisive factor in determining the THz propagation in the proposed fiber.

IV. Experimental Verification Using THz Spectroscopy

For experimental characterization of the porous fiber, we performed transmission measurements with the THz-TDS system, as shown in Fig. 2(a). The THz pulse in Fig. 5(a) is the reference signal that passes through a circular aperture with a hole diameter of 3 mm. The experimentally measured pulses after propagating through the proposed porous fibers

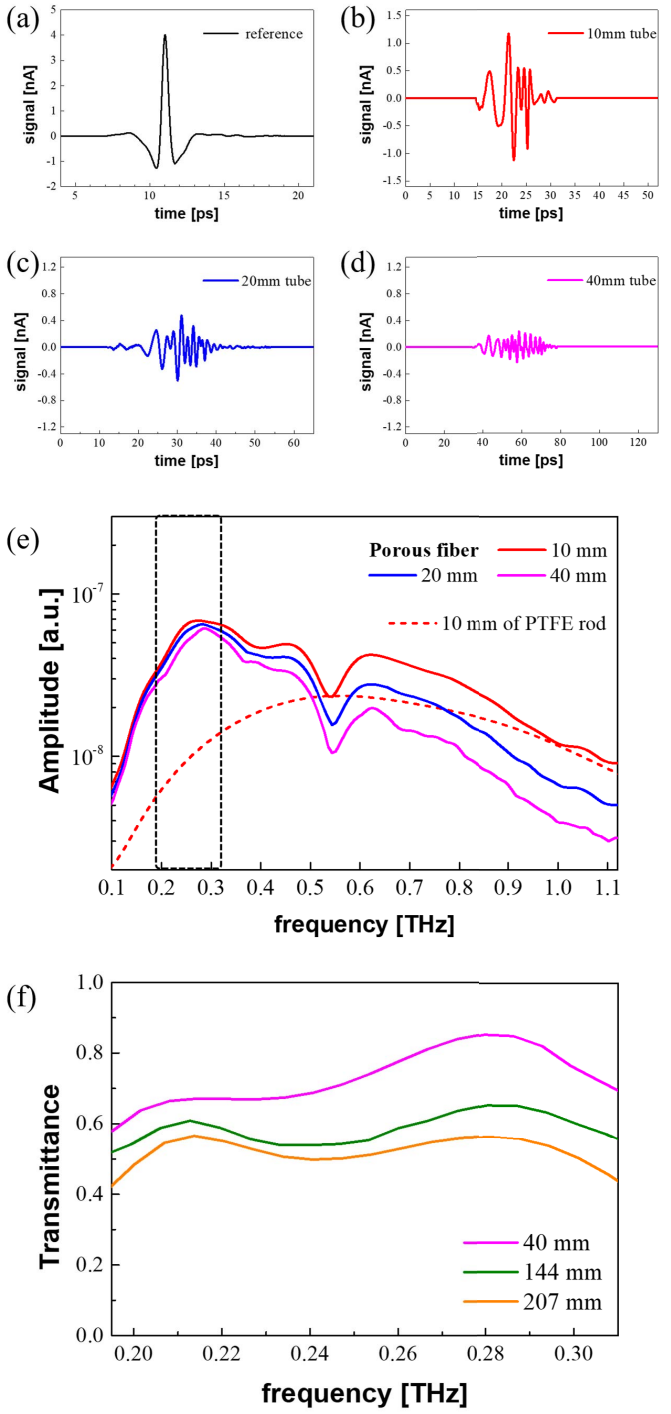

Fig. 5. Measured THz pulses for (a) reference signal (black curve) and (b) transmitted pulse through a 10-mm-long porous fiber (red curve), (c) 20-mm-long porous fiber (blue curve), and (d) 40-mm-long porous fiber (magenta curve). (e) Magnitude of the transmitted signals in the frequency domain. The red-dashed line is for the PTFE rod. (f) Transmittance depending on the length of 40, 144, and 207 mm.

with a length of 10, 20, and 40 mm are shown in Fig. 5(b)–(d), respectively. The transmitted THz waveform dispersed more in the time domain for the longer fiber length. Fig. 5(e) shows the magnitude of the transmitted signals in the frequency domain for both the proposed fibers and the PTFE rod with a length of 10 mm.

Experimentally, we observed that the proposed porous fiber showed a more significant transmission than the PTFE rod with the same O.D. by several factors, as in Fig. 5(e), which agreed well with the theoretical predictions to confirm the role of hexagonal air hole array to reduce EML. It is noteworthy that especially in the 6G band from 0.2 to 0.33 THz, almost an order of magnitude higher transmission was observed in our proposed fiber than the rod. This improvement is much better than the theoretical estimates in Fig. 3(a), which could be attributed to the scattering loss in the PTFE rod. In a higher frequency of over 0.5 THz, the proposed fiber did not show a significant advantage in EML reduction since the THz wave spread out of the air hole and is confined to the material edge of the fiber.

It is observed that a noticeable spectral dip exists between 0.5 and 0.6 THz. A similar spectral behavior has been observed in anti-resonant reflecting optical waveguides (ARROWs) [38] and the central air hole might have contributed internal reflection of the propagating THz wave as in ARROWs. There might be experimental attributes and we are investigating the origin of the spectral dip.

We experimentally estimated the transmittance of THz in the proposed fiber as in Fig. 5(f) for fiber lengths of 40, 144, and 207 mm in the 6G band. The magnitude of the signal passing through the aperture was taken as the reference. The proposed fibers of 40, 144, and 207 mm long showed a decent average transmittance of 71%, 59%, and 45%, respectively, the frequency range of interest.

Finally, we experimentally investigated the bending characteristics of the porous core fiber. Note that the PTFE porous fiber is susceptible to mechanical bending, which can alter the transmission characteristics. We defined the bending parameters shown in Fig. 6(a), the bending curvature C, and the bending direction θ. The bending curvature is expressed as

$$C = \frac{1}{R} = \frac{2h}{h^2 + d^2} \tag{4}$$

where the parameter, h, is the transverse displacement, and d is the distance between the fixed point and the point where the bending force is applied. When the bending direction is horizontal, θ is 0° as shown in the top-left of the inset of Fig. 6(a). If the bending direction is vertical, θ is 90°. See the bottom-right inset of Fig. 6(a). The insets show the fundamental mode intensity profiles calculated using FEM analysis for various bending conditions; $C = 3.1$ and 4.8 m^{-1} and $\theta = 0$ and 90°. For both bending directions, we expect that the fundamental mode shifted outward as C increases. Nevertheless, the proposed fiber still keeps a large overlap between the fundamental mode and the air holes. In bending experiments, the transmittance was measured directly by the frequency-domain system based on the photomixing CW THz source (TeraScan, TOPTICA) [39] and the Schottky diode detector from VDi [40]. The Schottky diode detector can measure the maximum amplitude of the THz signal passing through the optical fiber. The combination of CW source of

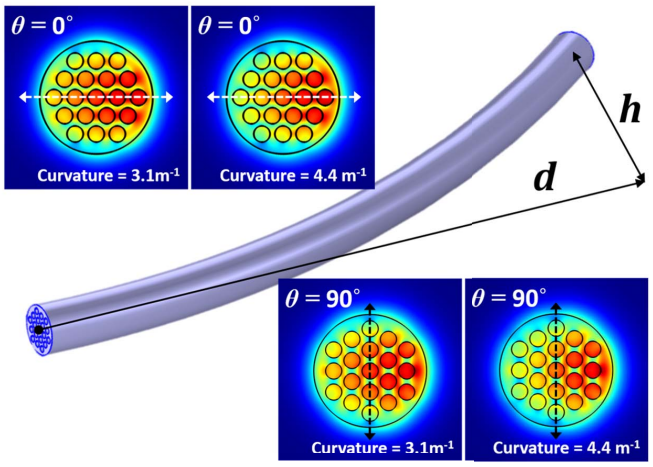

(a)

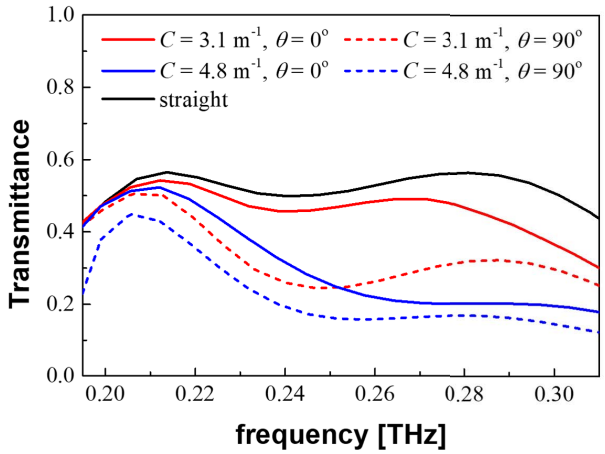

(b)

Fig. 6. Bent porous core fiber. (a) Schematic of the bending parameters in experiments and fundamental mode intensity distributions as a function of the curvature and bending direction angles. When the bending direction is horizontal, θ is 0. See the top-left in the inset. (b) Transmittance of the porous core fiber for various bending conditions, the curvature with $C = 3.1$ and 4.8 m^{-1}, and the bending direction of 0° and 90° in comparison to straight fiber.

Terascan and Schottky diode detector allowed more convenient bending experiments than the conventional THz-TDS system which is optimized for straight fibers. For various straight porous core fibers, we obtained the same transmittance in both measurement systems, the CW THz system and THz-TDS, to confirm the consistency of our measurements. Transmittance measurements through the bent porous core fiber are summarized in Fig. 6(b), for various bending parameters: $C = 3.1$ and 4.8 m^{-1} and $\theta = 0°$ and 90°. Here, transmission through a porous core fiber with a straight length of 207 mm was used as a reference. As the curvature increased, the transmittance decreased, especially in the high-frequency region $f > 0.22$ THz. In contrast, the frequency range near 0.21 THz showed a minor decrease in all bending conditions. It is also noted that the transmittance was affected by the bending direc-

TABLE I
COMPARISON OF THE PROPOSED POROUS CORE FIBER WITH PRIOR REPORTS

Reference	Structure/Dimension	Porosity	Material	EML	6G Transmittance ($0.2< f <0.33$ THz)	
					Straight	bending
Ref. [41]	Rectangular structure, O.D. = 300 μm, fiber length = 39 mm	65%	PMMA	< 0.25 cm^{-1} ($f < 0.8$)	-	-
Ref. [42]	Spider web structure, O.D. = 600 μm, fiber length = 25 mm	64%	COC	< 0.08 cm^{-1} ($0.2 < f < 0.35$)	-	-
Ref. [43]	Hexagonal structure, O.D. = 775 μm, fiber length = 38 cm	86%	PE	< 0.27 cm^{-1} ($0.18 < f < 0.30$)	45 ± 40 %	-
Ref. [44]	Hexagonal structure, O.D. = 1.35 mm fiber length = 18.5 cm	64%	LDPE	< 0.15 cm^{-1} ($0.3 < f < 1.5$)	-	-
This study	Hexagonal structure, O.D. = 3 mm fiber length = 207 mm	**40%**	PTFE	$<$ **0.07** cm^{-1} ($0.1 < f < 0.33$)	**45** ± 13 %	**40** ± 15 %

The unit of the frequency, f, is THz

TABLE II
COMPARISON OF THE EXPERIMENTALLY DEMONSTRATED REFERENCE AND THE PROPOSED FIBER

Reference	Material	Structure	Layer	Core diameter (O.D.)	Porosity	EML	Trasmission band	Transmittance at 0.3 THz
Ref. [43]	PE	Hexagonal	1	775 μm	86%	< 0.27 cm^{-1}	0.1 - 0.5 THz	30%*
Ref. [44]	LDPE	Hexagonal	4	1.47 mm	64%	< 0.15 cm^{-1}	0.3 - 1.5 THz	45%*
Ref. [45]	PMMA	Hexagonal	3	500 μm	74%	< 0.5 cm^{-1}*	0.2 - 0.8 THz	-
This study	PTFE	Hexagonal	2	3 mm	40%	< 0.07 cm^{-1}	**0.1 - 0.33 THz**	**50 %**

* represents estimation.

tion such that the fiber bending at $\theta = 90°$ showed a less transmittance than those at $\theta = 0°$. When $C = 3.1$ m^{-1} and $\theta = 0°$, the transmittance was 40 ± 15% at $f \sim 0.21$ THz, which was very close to 45 ± 13% of the straight reference fiber.

Table I shows a comparison of the proposed porous core fiber with the prior reports in terms of structure, EML, and 6G band transmission. The proposed porous fiber achieved the lowest EML and showed a stable transmittance even with bending in the 6G band, which has never been reported. PTFE has a slightly larger material absorption coefficient than COC, yet by an optimal air hole array structure, EML was reduced to the lowest level. PTFE can offer significantly versatile fabrication capability than COC to provide a uniform fiber length over 200 mm even with the largest O.D. of 3 mm, an order of magnitude longer fiber length than prior arts. The large O.D. effectively reduced the bending loss keeping the guided mode within the porous core maintaining a high level of air hole overlap. See Fig. 6(a).

In Table II, the proposed fibers are furthermore compared with porous core fibers having hexagonal symmetry in terms of the material, the air hole layer number, and the porosity. Using the large diameter with air holes arranged in two layers, our proposed fiber showed the highest transmission of 50% in 6G transmission band.

It is noteworthy that systematic numerical analyses summarized in Figs. 3(b) and 6 have not been attempted in prior reports. Especially, the bending experiments shown in Fig. 6 confirm the practical potentials of the proposed fiber in real environments where mechanical deformation is inevitable.

V. CONCLUSION

A defectless porous core fiber with hexagonally arranged air holes and its optical properties were investigated numerically and experimentally in the THz range. The fiber had an O.D. of 3.0 mm, a porosity of 40%, and a straight length of 207 mm. The numerical investigations predicted that the proposed porous core fiber provided a low EML from 0.02 to 0.07 cm^{-1} in the frequency range from 0.1 to 0.33 THz. Also, the proposed porous fiber minimizes the external influence by effectively reducing the power fraction in the air cladding.

In experiments, the fiber was found to have a 45 ± 13% transmittance in the potential 6G communication frequency band of 0.2–0.33 THz. The fiber also showed a good bending performance such that the transmittance was maintained at 40 ± 15% even when the fiber was bent at a curvature of $C = 3.1\ \mathrm{m}^{-1}$, which has not been achieved in prior arts. It is expected that the proposed fiber can be applied to make compact THz devices and systems by providing a high transmittance over a relatively long length over tens of centimeters under a relatively tight bending, such as communications and sensing in a low-frequency THz range.

REFERENCES

[1] R. Safian, G. Ghazi, and N. Mohammadian, "Review of photomixing continuous-wave terahertz systems and current application trends in terahertz domain," *Opt. Eng.*, vol. 58, no. 11, 2019, Art. no. 110901.

[2] J. A. Fülöp, S. Tzortzakis, and T. Kampfrath, "Laser-driven strong-field terahertz sources," *Adv. Opt. Mater.*, vol. 8, no. 3, Feb. 2020, Art. no. 1900681.

[3] L. Yu *et al.*, "The medical application of terahertz technology in non-invasive detection of cells and tissues: Opportunities and challenges," *RSC Adv.*, vol. 9, no. 17, pp. 9354–9363, 2019.

[4] R. B. Kohlhaas *et al.*, "Terahertz quasi time-domain spectroscopy based on telecom technology for 1550 nm," *Opt. Exp.*, vol. 25, no. 11, pp. 12851–12859, May 2017.

[5] J.-H. Son, S. J. Oh, and H. Cheon, "Potential clinical applications of terahertz radiation," *J. Appl. Phys.*, vol. 125, no. 19, May 2019, Art. no. 190901.

[6] K. Tekbıyık, A. R. Ekti, G. K. Kurt, and A. Görçin, "Terahertz band communication systems: Challenges, novelties and standardization efforts," *Phys. Commun.*, vol. 35, Aug. 2019, Art. no. 100700.

[7] *IEEE 802.15 3D, IEEE Standard for High Data Rate Wireless Multi-Media Networks—Amendment 2: 100 Gb/s Wireless Switched Point-to-Point Physical Layer*, IEEE Standard 802.15.3d-2017, Jan. 2017, pp. 1–55.

[8] V. Petrov *et al.*, "On unified vehicular communications and radar sensing in millimeter-wave and low terahertz bands," *IEEE Wireless Commun.*, vol. 26, no. 3, pp. 146–153, Jun. 2019.

[9] W. Volkaerts, N. Van Thienen, and P. Reynaert, "An FSK plastic waveguide communication link in 40nm CMOS," in *IEEE Int. Solid-State Circuits Conf. (ISSCC) Dig. Tech. Papers*, Feb. 2015, pp. 178–179.

[10] Q. Zhong, Z. Chen, N. Sharma, S. Kshattry, W. Choi, and K. O. Kenneth, "300-GHz CMOS QPSK transmitter for 30-gbps dielectric waveguide communication," in *Proc. IEEE Custom Integr. Circuits Conf. (CICC)*, Apr. 2018, pp. 1–4.

[11] P. Reynaert *et al.*, "Polymer microwave fibers: A blend of RF, copper and optical communication," in *Proc. IEEE ESSCIRC*, Sep. 2016, pp. 15–20.

[12] M. Wächter, M. Nagel, and H. Kurz, "Metallic slit waveguide for dispersion-free low-loss terahertz signal transmission," *Appl. Phys. Lett.*, vol. 90, no. 6, Feb. 2007, Art. no. 061111.

[13] J. S. Jo and T.-I. Jeon, "Characteristics of THz pulse propagation on Teflon covered two-wire lines," *J. Opt. Soc. Korea*, vol. 19, no. 6, pp. 560–565, Dec. 2015.

[14] B. Bowden, J. A. Harringto, and O. Mitrofanov, "Silver/polystyrene-coated hollow glass waveguides for the transmission of terahertz radiation," *Opt. Lett.*, vol. 32, no. 20, pp. 2945–2947, 2007.

[15] S. Kim, Y. S. Lee, C.-S. Kee, and C. G. Lee, "Dispersion flattened terahertz photonic crystal fiber with high birefringence and low confinement loss," *Proc. SPIE, THz, RF, Millim., Submillim.-Wave Technol. Appl. VII*, vol. 8985, Mar. 2014, Art. no. 89851L.

[16] G. Zhao, M. T. Mors, and T. Wenckebach, "Terahertz dielectric properties of polystyrene foam," *J. Opt. Soc. Amer. B, Opt. Phys.*, vol. 19, no. 6, pp. 1476–1479, 2007.

[17] J.-Y. Lu *et al.*, "Terahertz air-core microstructure fiber," *Appl. Phys. Lett.*, vol. 92, no. 6, Feb. 2008, Art. no. 064105.

[18] W. Talataisong *et al.*, "Novel method for manufacturing optical fiber: Extrusion and drawing of microstructured polymer optical fibers from a 3D printer," *Opt. Exp.*, vol. 26, no. 24, pp. 32007–32013, 2018.

[19] H. Pakarzadeh, S. M. Rezaei, and L. Namroodi, "Hollow-core photonic crystal fibers for efficient terahertz transmission," *Opt. Commun.*, vol. 433, no. 15, pp. 81–88, Feb. 2019.

[20] S. Atakaramians, S. Afshar V., T. M. Monro, and D. Abbott, "Terahertz dielectric waveguides," *Adv. Opt. Photon.*, vol. 5, no. 2, pp. 169–215, Jun. 2013.

[21] I. K. Yakasai, P. E. Abas, and F. Begum, "Review of porous core photonic crystal fibers for terahertz waveguiding," *Optik*, vol. 229, Mar. 2021, Art. no. 166284.

[22] A. Hassani, A. Dupuis, and M. Skorobogatiy, "Low loss porous terahertz fibers containing multiple subwavelength holes," *Appl. Phys. Lett.*, vol. 92, no. 7, Feb. 2008, Art. no. 071101.

[23] A. Habib and S. Anower, "Low loss highly birefringent porous core fiber for single mode terahertz wave guidance," *Curr. Opt. Photon.*, vol. 2, no. 3, pp. 215–220, 2018.

[24] A. Hassani, A. Dupuis, and M. Skorobogatiy, "Porous polymer fibers for low-loss terahertz guiding," *Opt. Exp.*, vol. 16, no. 9, pp. 6340–6351, 2008.

[25] J. Sultana *et al.*, "Highly birefringent elliptical core photonic crystal fiber for terahertz application," *Opt. Commun.*, vol. 407, no. 15, pp. 92–96, Jan. 2018.

[26] M. Goto, A. Quema, H. Takahashi, S. Ono, and N. Sarukura, "Teflon photonic crystal fiber as terahertz waveguide," *J. Appl. Phys.*, vol. 43, no. 2B, pp. 317–319, 2004.

[27] T. Yang, E. Wang, H. Jiang, Z. Hu, and K. Xie, "High birefringence photonic crystal fiber with high nonlinearity and low confinement loss," *Opt. Exp.*, vol. 23, no. 7, pp. 8329–8337, 2015.

[28] F. Distler, M. Sippel, J. Schür, G. Gold, K. Helmreich, and M. Vossiek, "Additively manufactured dielectric waveguides for advanced concepts for millimeter-wave interconnects," *IEEE Trans. Microw. Theory Techn.*, vol. 67, no. 11, pp. 4298–4307, Nov. 2019.

[29] F. Distler, M. Vossiek, and J. Schür, "Novel dielectric waveguide design studies for mmW applications," in *Proc. Asia–Pacific Microw. Conf. (APMC)*, Nov. 2018, pp. 288–290, Paper WE1-IF-12.

[30] H. Ebendorff-Heidepriem and T. M. Monro, "Extrusion of complex preforms for microstructured optical fibers," *Opt. Exp.*, vol. 15, no. 23, pp. 15086–15092, 2007.

[31] *Zeusinc*. Accessed: Jun. 20, 2018. [Online]. Available: https://www.zeusinc.com/

[32] H. Bao, K. Nielsen, H. K. Rasmussen, P. U. Jepsen, and O. Bang, "Fabrication and characterization of porous-core honeycomb bandgap THz fibers," *Opt. Exp.*, vol. 20, no. 28, pp. 29507–29517, Dec. 2012.

[33] Y. Zhang, L. Xue, D. Qiao, and Z. Guang, "Porous photonic-crystal fiber with near-zero ultra-flattened dispersion and high birefringence for polarization-maintaining terahertz transmission," *Optik*, vol. 207, Apr. 2020, Art. no. 163817.

[34] J. Neu and C. A. Schmuttenmaer, "Tutorial: An introduction to terahertz time domain spectroscopy (THz-TDS)," *J. Appl. Phys.*, vol. 124, no. 23, Dec. 2018, Art. no. 231101.

[35] A. Krotkus, "Semiconductors for terahertz photonics applications," *J. Phys. D, Appl. Phys.*, vol. 43, no. 27, Jul. 2010, Art. no. 273001.

[36] H. K. Yoo *et al.*, "Organic conjugated material-based broadband terahertz wave modulators," *Appl. Phys. Lett.*, vol. 99, no. 6, Aug. 2011, Art. no. 061108.

[37] M. Faisal and M. S. Islam, "Extremely high birefringent terahertz fiber using a suspended elliptic core with slotted airholes," *Appl. Opt.*, vol. 57, no. 13, pp. 3340–3347, 2018.

[38] L. D. van Putten, J. Gorecki, E. N. Fokoua, V. Apostolopoulos, and F. Poletti, "3D-printed polymer antiresonant waveguides for short-reach terahertz applications," *Appl. Opt.*, vol. 57, no. 14, pp. 3953–3958, 2018.

[39] *TOPTICA*. Accessed: Apr. 1, 2020. [Online]. Available: https://www.toptica.com/

[40] *Virginia Diodes Inc.* Accessed: Apr. 1, 2020. [Online]. Available: https://www.vadiodes.com/

[41] S. Atakaramians *et al.*, "THz porous fibers: Design, fabrication and experimental characterization," *Opt. Exp.*, vol. 17, no. 16, pp. 14053–14062, Jul. 2009.

[42] S. Atakaramians *et al.*, "Direct probing of evanescent field for characterization of porous terahertz fibers," *Appl. Phys. Lett.*, vol. 98, no. 12, Mar. 2011, Art. no. 121104.

[43] A. Dupuis, A. Mazhorova, F. Désévédavy, M. Rozé, and M. Skorobogatiy, "Spectral characterization of porous dielectric subwavelength THz fibers fabricated using a microstructured molding technique," *Opt. Exp.*, vol. 18, no. 13, pp. 13813–13828, 2010.

[44] T. Ma, A. Markov, L. Wang, and M. Skorobogatiy, "Graded index porous optical fibers—Dispersion management in terahertz range," *Opt. Exp.*, vol. 23, no. 6, pp. 7856–7869, 2015.

[45] S. Atakramians, S. Afshar, B. M. Fischer, D. Abbott, and T. M. Monro, "Porous fibers: A novel approach to low loss THz waveguides," *Opt. Exp.*, vol. 16, no. 12, pp. 8845–8854, 2008.